Regulation of the essential peptidoglycan hydrolytic complex FtsEX-PcsB during *Streptococcus pneumoniae* cell division

Nicholas S Briggs[1*], Kevin E Bruce[2], Stefano Camaione[1], Souvik Naskar[1,3], Adrian Lloyd[1], Malcolm E Winkler[2] & David I Roper[1*]

[1] School of Life Sciences, University of Warwick, Coventry, CV4 7AL, UK

[2]Department of Biology, Indiana University Bloomington, Bloomington, IN 47405, USA

[3]Imperial College London, South Kensington, London SW7 2BX

* To whom correspondence should be addressed. Nicholas S Briggs, School of Life Sciences, University of Warwick, CV4 7AL, nicholas.s.briggs@warwick.ac.uk

David I Roper, School of Life Science, University of Warwick, CV4 7AL, +44 (0) 2476528369, david.roper@warwick.ac.uk

Classification:

- Major – Biological Sciences
- Minor – Biochemistry

Keywords: PEPTIDOGLYCAN | PNEUMOCOCCUS | CELL DIVISION | HYDROLASE |

Significance Statement

Bacterial cell division requires coordinated assembly of specific proteins acting on the cell envelope to induce division. The cell division complex FtsEX is recruited early in divisome assembly and controls extracellular hydrolase function, which modifies the peptidoglycan layer. We demonstrate in *Streptococcus pneumoniae*, where these proteins are essential, connections between ATP hydrolysis in cytosolic FtsE, mechanotransduction through FtsX in the membrane, activation of PcsB in the intracellular space and molecular details of the chemical modification of the peptidoglycan layer. Here we present a model whereby the FtsEX-PcsB complex is assembled early in order to produce a hydrolase-modified form of peptidoglycan during septal splitting, marking the site of later division events; thus providing a rationale for its biological and temporal function.

Abstract

In the human commensal Gram-positive bacterial pathogen *Streptococcus pneumoniae,* the essential extracellular cell-division-associated peptidoglycan (PG) hydrolase PcsB interacts directly with the cytoplasmic-membrane-bound complex between FtsE and FtsX (1–3). PcsB contains a cysteine, histidine-dependent amidohydrolase/peptidase (CHAP) domain responsible for PG hydrolysis, as well as a coiled-coil domain required for interaction with FtsEX (1,4). ATP hydrolysis of FtsE in the cytoplasm drives conformational changes in FtsX in the cytoplasmic membrane, which ultimately regulates the PG hydrolase on the outside of the cell (5). In this work we show using *in vitro* and *in vivo* approaches, that the CHAP domain of PcsB predominately functions as an *iso*-D-Glutaminyl-Lysyl D,L-endopeptidase, with particular substrate specificity for Lys-containing, amidated PG, cleaving between the second and third amino acids of the peptidoglycan stem peptide. The catalytic activity of PcsB is regulated and activated by conformation changes of the coiled-coil region of PcsB and in part by a short helical region immediately adjacent to the CHAP domain to guard against PcsB hydrolytic activation outside of its cell division specific functional requirement. This work supports a model for the overall biological activity of the FtsEX-PcsB complex, in which ATP hydrolysis by FtsE in the cytoplasm, drives conformational changes in FtsX and PcsB resulting in the liberation of the hydrolytic CHAP domain of PcsB from its regulatory helix to allow PG stem peptide cleavage that splits the septal disk and marks a region of the peptidoglycan sacculus for subsequent cell division remodelling.

Introduction

Cell division represents one the most fundamental and complex processes undertaken by a bacterial cell. Central to this process is turnover of the bacterial cell wall structural polymer peptidoglycan to enable separation of individual cells (6,7). During cell division, selected conserved proteins dynamically facilitate alterations to membrane and cell wall morphology, enabling coordination between events located on both the inside and outside of the cytoplasmic membrane (7). Previous studies of bacterial cell morphology in *Escherichia coli* (8,9) and *Bacillus subtilis* (10–12) in particular, have identified key proteins and complexes required for division using detailed genetic, biochemical, and advanced microscopy techniques. Homologues of many of the key cell division proteins are found in almost all

63 bacterial species, that importantly underline their essentiality and common genetic origin
64 (7,8,13,14).
65
66 In the early stages of bacterial cell division, a complex between the FtsE and FtsX (FtsEX)
67 proteins is formed (1,5,15,16) and is recruited via interaction with the filament-forming
68 proteins FtsA and FtsZ to form components of the cytoplasmic Z-ring (17,18). The Z-ring
69 provides the foundation for the later assembly of a complex termed the bacterial divisome
70 (7,8,19) which accomplishes the process of cell division. FtsX is an integral membrane protein
71 which forms a dimer and partners with a dimer of FtsE, the cytoplasmic nucleotide-binding
72 domain of the FtsEX complex. The FtsEX complex is an important member of the early
73 divisome apparatus mediating important protein-protein interactions and also has a direct
74 role in controlling PG degradation activity via extracellular hydrolytic proteins
75 (5,15,16,20). Whilst FtsEX is a structural homologue of the type VII family of ATP dependent
76 ABC transporters, it has no transport role but instead uses ATP hydrolysis in FtsE to transduce
77 a signal through FtsX to extracellular partner proteins to bring about controlled PG
78 degradation (5,15,16,20,21).
79
80 In rod-shaped Gram-negative bacteria including *E.coli*, FtsEX is not essential but is required
81 for viability in low-osmolarity media (20). By contrast, FtsEX and its PG hydrolase binding
82 partner PcsB are essential in the ovoid-shaped Gram-positive bacteria *Streptococcus*
83 *pneumoniae* (*Spn* or pneumococcus). Gram-positive and Gram-negative bacterial FtsEX
84 complexes are also further delineated by their relationship to the cognate PG hydrolases
85 which they activate and control. In typical Gram-negative bacterial species such as *E. coli*, the
86 FtsEX protein complex binds to a structural, regulatory coiled-coil protein EnvC , which itself
87 has no enzymatic activity, but in turn binds to and regulates the activity of one or a series of
88 zinc-dependent PG amidase enzymes (AmiA, AmiB) in order to degrade the PG (22,23). In
89 contrast, Gram-positive bacteria such as *B. subtilis* and *S. pneumoniae* have a direct
90 relationship, in which the structural regulator protein and enzymatic PG hydrolase are within
91 a single protein such as CwlO (21,24) or PcsB (1,4) respectively. Why Gram-negative species
92 like *E.coli* and *Pseudomonas aeruginosa* have alternative PG hydrolytic warheads
93 (AmiA/AmiB) whose association with FtsEX requires an adaptor protein (EnvC) and what

94 determines their selection, remains an unexplored area but may be linked to the great
95 compartmentalised structure of the Gram-negative cell envelope.
96
97 It has been shown previously that the full-length *S. pneumoniae* PcsB protein displays no
98 hydrolytic activity *in vitro* until the N-terminal coiled-coil region of the protein is removed (4),
99 suggesting a critical conformational regulatory function is required for PcsB PG hydrolytic
100 activation. The remaining C-terminal section of PcsB is a cysteine, histidine-dependent
101 amidohydrolase/peptidase (CHAP) domain that shares overall homology to other PG
102 hydrolases (16,21,24), and thus was assumed to play a similar role to that of the *E. coli*
103 amidases during cell division which target the MurNAc-L-Ala bond to produce fully denuded
104 glycan strands (23,25). However, PcsB has no metal dependency and has closer homology to
105 other Gram-positive PG hydrolases like the *B. subtilis* DL-endopeptidase CwlO (21). However,
106 little is known about PcsB's *in vivo* target bond and product and how this relates to the
107 essential role it plays during cell division.
108
109 The X-ray crystal structure of the full-length PcsB protein revealed a dimeric head-to-head
110 arrangement of the CHAP domains that prevented PG degradation activity (4), but
111 biochemical studies revealed the activity of the CHAP domain in isolation. Subsequent studies
112 on the structures of *E.coli* EnvC-AmiA/B (23) as well as the complexes of *P.aeruginosa* FtsX-
113 EnvC, *P.aeruginosa* FtsEX-EnvC-AmiB (26), *Vibrio cholerae* FtsEX-EnvC (15)**,** *M. tuberculosis*
114 FtsEX-RipC (16) and *E.coli* FtsEX-EnvC (5) have revealed structural arrangements of the FtsEX
115 heterodimer complex with a single extracellular binding partner which are the subject of a
116 recent review (27). In total we now have a collective understanding of FtsEX function as
117 enabling a conformational change in the extracellular hydrolase protein, presumably to
118 position the hydrolase active site within the PG target layer as well as structural elements
119 adjacent to the hydrolase that control hydrolytic activity.
120
121 It is worth noting when considering the peptidoglycan layer in *S.pneumoniae* that it is made
122 of direct and indirect cross links in which the side chain of Lys at the third position of the
123 peptide stem can be modified with L-Ser-L-Ala or D-Ala-L-Ala (as a result of amino acyl-tRNA
124 dependent MurM and MurN action (28–30)). Altered stem peptide content and the resulting
125 increase in PBP-mediated indirect crosslinking is found in highly-penicillin-resistant strains

126 (31). A recent report of the catalytic domain of non-essential VldE (Spr1875) shows it to be a
127 zinc-dependent L-D-endopeptidase which hydrolyses the cross-linked stem peptide and is
128 induced via the VicRK (WalRK) two component system under stress conditions (32), as is PcsB
129 (33,34) . Unlike previously mentioned PG amidases, VldE can produce a form of PG in which
130 the first L-alanine in the peptide stem is left attached to the glycan sugar backbone (the
131 hydrolysed bond is between L-Ala and D-Glu on the non-amidated synthetic peptides tested)
132 (32). The role of VldE, which cannot replace PcsB, is unknown, but may be stress related (32).
133 The LytA protein of *S.pneumoniae*, which is an *N*-acetylmuramoyl-l-alanine amidase produced
134 in the cytoplasm, produces a fully denuded glycan strand but appears to play a role in
135 fratricidal stress-induced lysis rather than in cell division (35).
136
137 In this study, we explore the structure-function relationship between the *S.pneumoniae* FtsEX
138 complex with PcsB using *in-vitro* and *in-vivo* approaches that seek to explore the biological
139 events that control PG hydrolysis. We explore the substrate specificity of $PcsB_{CHAP}$ whilst
140 elucidating the molecular target and product of PcsB's activity, defining the chemical nature
141 of the hydrolase-modified PG following PcsB CHAP domain action. Finally, we demonstrate a
142 putative regulatory element of $PcsB_{CHAP}$ which is FtsX-independent, providing additional
143 regulation of the tightly-controlled FtsEX-PcsB PG hydrolytic activity..
144

145 # Results

146 **Co-overexpression of *Spn* PcsB and *Spn* FtsEX rescues phenotypic defects observed**
147 **in *E. coli* when *Spn* FtsEX is overexpressed in isolation**

148 We began our investigations by building on previous work in which an *ftsEX* knockout in *E.*
149 *coli* demonstrated poor growth and cell death under osmotic stress conditions (18,36–
150 38). Whilst the direct role of these proteins in *E. coli* in relation to stress is still unclear, the
151 phenotype can be used as a tool for complementation experiments. Using an *ftsEX* knockout
152 strain of *E. coli* (BW25113 Δ*ftsEX*) we tested the viability of cells on rich (LB) or stress (LB
153 without NaCl, LB0N) solid media supplemented with 1mM IPTG in a spot titre assay (Supp Fig.
154 1). Under osmotic stress, the Δ*ftsEX* strain barely supports growth, but can be complemented
155 by pneumococcal *ftsEX* expression from the gene cassette in our pET-DUET vector construct,
156 (Supplementary Table 2) by more than two orders of magnitude (Supp Fig. 1B). *E. coli*

157 BW25113 has no DE3 T7 RNA polymerase system so expression may be at a basal level from
158 recognition of *E. coli* RNA polymerase of the plasmid promoter system. Notably, this suggests
159 a shared role for FtsEX across multiple organisms, and suggests a functional role for
160 pneumococcal FtsEX in an *E. coli* host environment under low-salt conditions.
161
162 Given the essentiality of these genes in *S. pneumoniae,* we next chose to express these
163 proteins in an *E. coli* heterologous expression system, in which wild-type expression levels of
164 *E. coli* FtsEX-EnvC-AmiAB are assumed. This system also allows testing of the individual
165 components of the FtsEX-PcsB complex. The *pcsB* gene was separately cloned into a pCDF-
166 DUET vector downstream of a *pelB* leader sequence (to enable the protein to be directed into
167 the *E. coli* periplasm) also under T7 promoter control (Supplementary Table 2), to allow co-
168 transformation and heterologous expression of FtsEX-PcsB as a functional complex or as
169 individual components in *E. coli*. Preliminary experiments suggested overexpression of *Spn*
170 FtsEX at late log phase resulted in a large proportion of highly filamentous *E. coli* cells, with
171 no defined division septa along their length. To explore this in more detail, cells were
172 synchronised using DL-serine hydroxamate (39) prior to protein expression and grown to late-
173 log/stationary phase in order to visualise phenotypic effects due to the presence of the
174 recombinant proteins, rather than the transient effects of protein overexpression *per se* (40–
175 42). The filamentous phenotype was reproduced during *Spn* FtsEX overexpression under
176 these conditions (Fig. 1B) but not with *Spn* PcsB in isolation (Supp Fig. 2G). By contrast, when
177 PcsB was expressed in addition to FtsEX, the cells reverted to a rod-shaped phenotype (Fig.
178 1C). This unexpected but dramatic observation is consistent with FtsEX-PcsB acting in a
179 functional manner during *E. coli* growth and division, rather than a more general non-specific
180 effect of protein expression. The presence of PcsB within the context of the FtsEX-PcsB
181 complex is apparently able to rescue the cell-division defect phenotype observed when FtsEX
182 is overexpressed in isolation therefore.
183

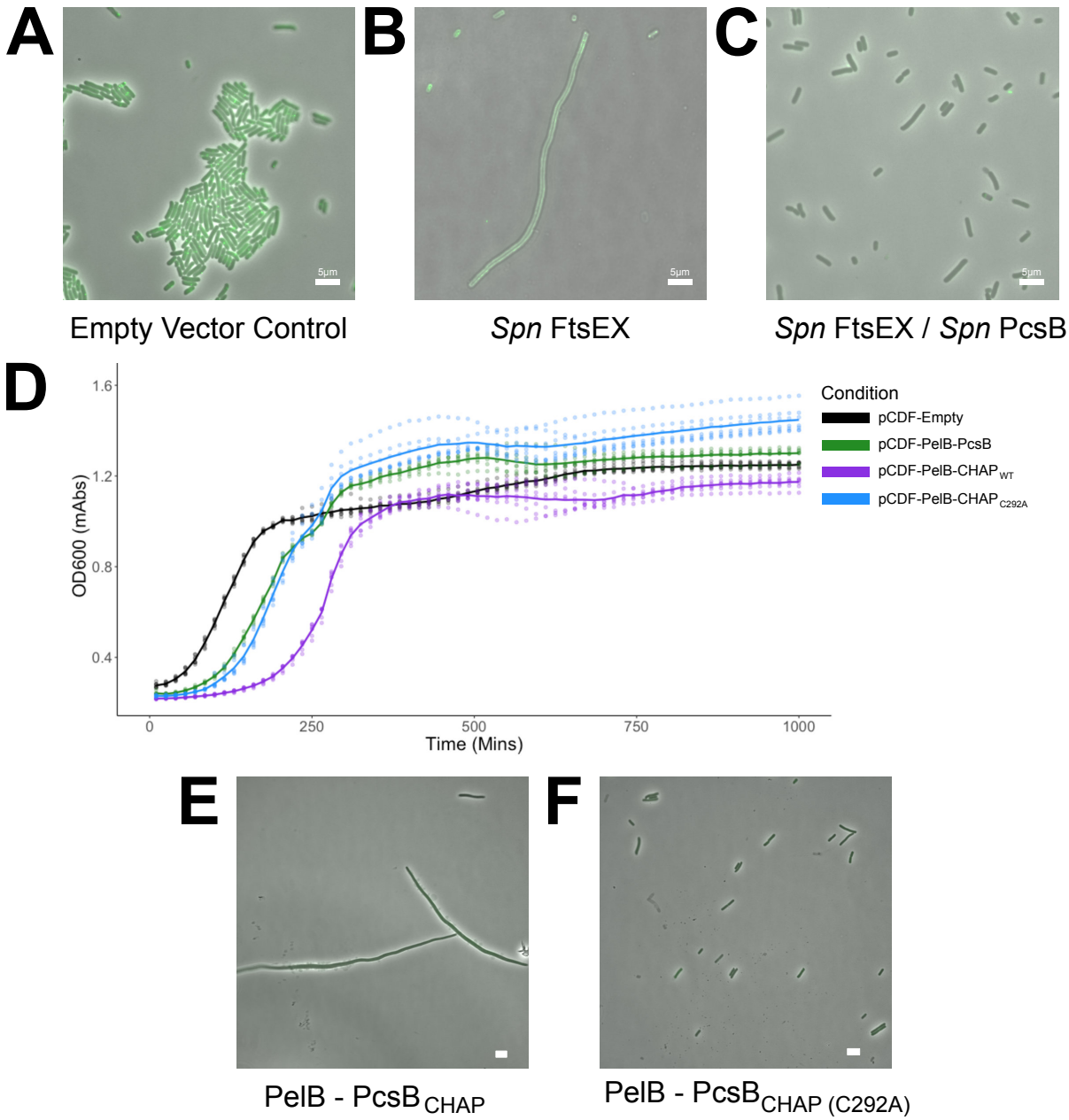

Figure 1 - Co-overexpression of pneumococcal PcsB with pneumococcal FtsEX rescues the filamentous phenotype of FtsEX alone in *E. coli,* however overexpression of the PcsB CHAP domain in isolation forms filaments as well. A strain of BL21 *E. coli* in which the parental *ftsZ* gene is tagged with mNEON was used to visualise division septa during overexpression of pneumococcal proteins. Both empty vector (A) and FtsEX-PcsB (C) induced normal, rod-shaped *E. coli*, whereas expression of FtsEX alone induced filamentous cells (B). Growth curves of *E. coli* overexpressing empty vector, WT PcsB, PcsB CHAP domain or inactive PcsB CHAP (C292A) in the periplasm (PelB leader) (D) alongside representative microscopy images of active CHAP domain (E) or inactive CHAP domain (F) demonstrating cell division defects when the unregulated CHAP domain is active. Points mark OD reading at each time point, line marks best fit line. Magnification of 100x.

196 **Exploring the structure-activity relationship of the FtsEX-PcsB complex.**

197 In order to investigate these observations further and examine FtsEX-PcsB's dependency on
198 ATP turnover for activity, we explored whether the cell-shape phenotype was dependent on
199 the ATPase activity of FtsE within this complex, given the homology of the FtsEX-PcsB complex
200 to ATP-dependent ABC transporters. Mutations were made in the Walker A and B motifs of
201 the *ftsE* gene to disrupt β-phosphate stabilisation (K43A) or Mg^{2+} binding (E165Q), as well as
202 to the adenosine pi-stacking residue (Y13A); these mutants and FtsX were overexpressed in
203 *E. coli* in the presence and absence of PcsB (Supp Fig 2). All three individual mutations
204 resulted in the same filamentous phenotype response as wild-type FtsEX when expressed in
205 isolation or with PcsB (Supp Table 5), implying that the fully functional FtsEX-PcsB complex
206 (including the PG hydrolytic activity of PcsB) is required for cell division in *E. coli* when the
207 proteins are being overexpressed. It should be noted that the proportion of cells that become
208 filamentous is reduced with the mutant *Spn* FtsEX overexpression (Supp Fig 2). This could be
209 due to compensatory mechanisms overcoming the deleterious effects that *Spn* FtsEX
210 produces; or decreased induction of these proteins over time. We extended our phenotypic
211 study to investigate if the PG hydrolytic activity of PcsB was also required to rescue the
212 filamentous FtsEX-induced phenotype. An active-site Cys to Ala (C292A) mutant of *pcsB* was
213 constructed and tested in the heterologous expression system (Supp Fig. 2 and Supp Table
214 5). This showed that overexpression of $PcsB_{C292A}$ in the presence of wild-type FtsEX did not
215 rescue filamentation to rod-shaped cells (Supp Table 5). Overexpression of either PcsB wild-
216 type or C292A without *Spn* FtsEX has no obvious phenotypic effect in *E. coli* (Supp Fig. 2 and
217 Supp Table 5).

218

219 To further investigate the structural elements required for the PG hydrolytic activity of PcsB,
220 and specifically the CHAP domain of this protein, we cloned and expressed a variety of
221 constructs. In addition to the full-length wild-type and C292A mutant PcsB constructs
222 (detailed above), we made a truncated PcsB construct in which only the CHAP domain is
223 directly preceded by a PelB leader sequence, thereby eliminating all proposed regulatory
224 elements of the protein encompassed within the coiled-coil region ($PcsB_{CHAP}$). Comparison of
225 growth between *E. coli* overexpressing empty-vector, $PcsB_{CHAP}$, $PcsB_{CHAP\ (C292A)}$ and $PcsB_{WT}$
226 cells showed a slight increase in the time taken to enter exponential phase for both the

227 catalytically inactive $PcsB_{CHAP\ (C292A)}$ and $PcsB_{WT}$ compared to the empty-vector cells. This
228 effect is exacerbated with the $PcsB_{CHAP}$ overexpression condition, indicating the active
229 hydrolase has an aberrant effect on growth (Fig. 1 D). Phenotypic analysis of these cells
230 revealed the $PcsB_{CHAP}$ overexpression induces the same apparent phenotype as wild-type
231 FtsEX, indicating the isolated hydrolase, lacking the proposed regulatory elements of the
232 coiled-coil domain, induces cell division defects (Fig. 1 E and F).
233

234 **The CHAP domain of PcsB ($PcsB_{CHAP}$) is an *iso*Glutaminyl-Lysyl DL-endopeptidase.**

235 We conducted a series of structure-function experiments in order to understand the
236 peptidoglycan hydrolysis activity of PcsB at a molecular level. We expressed and purified the
237 CHAP domain of PcsB (A274-D392, $PcsB_{CHAP}$) in order to explore its enzyme activity devoid of
238 regulatory or inhibitory elements (Supp Fig 3). Initially we explored the activity of $PcsB_{CHAP}$
239 against whole peptidoglycan isolated from *S. pneumoniae* cells in which the enzymatic
240 breakdown of the complex polymer was monitored by decreases in absorbance at either 206
241 nm or 254 nm wavelengths to detect peptidase activity by carboxyl generation or glycan-
242 strand cleavage, respectively (43). Lysozyme and recombinantly expressed pneumococcal
243 LytA (Fig. 2A, B, Supp Fig 3B and 4) act as controls for each detection wavelength due to their
244 well characterised endoglycosidase or endopeptidase activity respectively
245 (35,44,45). Visualisation of the fold change of absorbance before and after the addition of
246 protein (Fig. 2A and B, Supp. Fig. 4) demonstrates $PcsB_{CHAP}$ displays comparatively high levels
247 of activity at 206 nm (Fig. 2A), but minimal activity at 254 nm (Fig. 2B), consistent with
248 hydrolytic activity upon the peptide stem rather than the glycan backbone. Recombinantly
249 expressed and purified $PcsB_{WT}$ and $PcsB_{CHAP\ (C292A)}$ as well as natively expressed PcsB secreted
250 and purified from pneumococcal cultures (Supp Fig 4) showed virtually no activity at either
251 wavelength (Fig. 2 A and B). This is consistent with the hypothesis that PcsB is only active
252 within the context of the FtsEX-PcsB complex during division (4).
253 We aimed to further dissect the endopeptidase chemical specificity of $PcsB_{CHAP}$ relative to the
254 PG polymer in *S. pneumoniae*. We purified additional PG substrates from *E. coli*, *M. leutus*
255 and *M. smegmatis*, providing the major variations in stem peptide combinations at positions
256 two and three: iso-D-Gln-Lys (*Spn*), D-Glu-diaminopimelic acid (DAP; *E. coli*), D-Glu-Lys (*M.*
257 *leutus*), *iso*-D-Gln-DAP (*M. smegmatis*) (46–48). Using these as PG substrates in the light

258 scattering assay as described previously, we were able to ascertain that the *iso*Gln-Lys-
259 containing substrate, as found in *S. pneumoniae*, was the preferred substrate over a D-Glu-
260 Lys-containing substrate, as found in *M. luteus* (Fig. 2C and 3). The DAP-containing PG stems
261 found in *E. coli* and *M. smegmatis* were significantly poorer substrates in the assay
262 irrespective of the amidation of the second position amino acid but notably still acted as
263 substrates, as shown by phenotypic changes in overexpressing cells (Fig. 1E); though this
264 effect is only seen over a much greater time period. This indicates a wide substrate tolerance
265 for the $PcsB_{CHAP}$ active site.
266

267

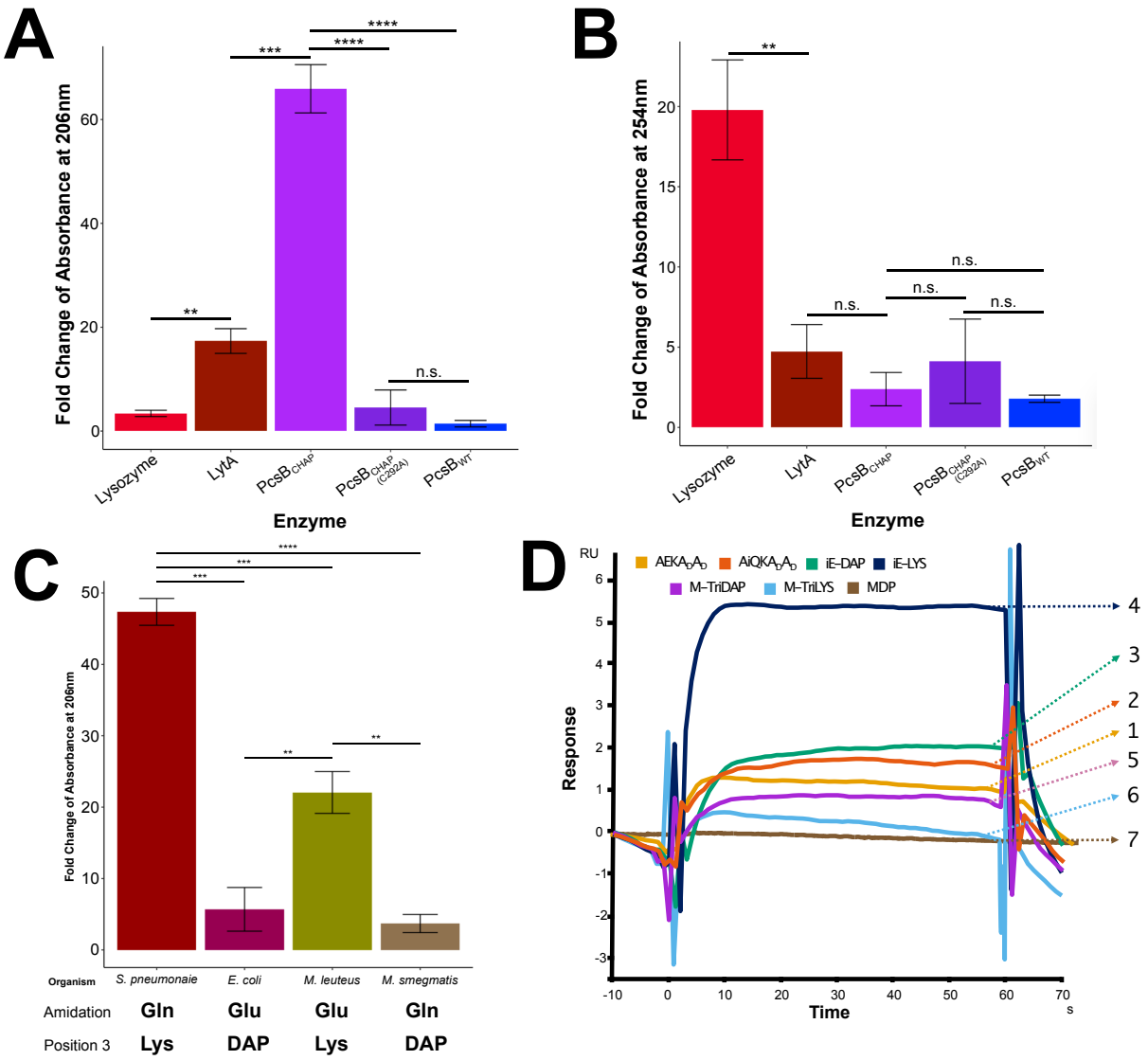

E

Analyte	k_a (1/Ms)	k_d (1/s)	R_{max} (RU)	KD (M)
1. AEKA$_D$A$_D$	3.33×10^{4}	3.60×10^{-2}	13.7	1.09×10^{-6}
2. AiQKA$_D$A$_D$	9.96×10^{4}	5.02×10^{-3}	0.169	5.05×10^{-8}*
3. iE-DAP	1.58×10^{5}	1.7×10^{-2}	18.5	1.13×10^{-7}
4. iE-LYS	1.02×10^{5}	9.56×10^{-3}	20.44	9.41×10^{-8}
5. M-TriDAP	6.28×10^{3}	3.94×10^{-3}	67.59	6.27×10^{-7}*
6. M-TriLYS	9.82×10^{4}	1.17×10^{-2}	0.074	1.19×10^{-7}*
7. MDP	4.27×10^{5}	5.03×10^{-2}	0.138	Not applicable

268

269 **Figure 2 – PcsB$_{CHAP}$ displays endopeptidase activity with specificity for amidated, Lys-containing**
270 **peptidoglycan substrates, cleaving between the *iso*Gln-Lys bond.** Light scattering-based assay using
271 purified *Spn* peptidoglycan as a substrate measured at 206 nm (A) for carboxyl generation or 254 nm
272 (B) for glycosidic bond presence. Light scattering-based assay measured at 206 nm using PcsB$_{CHAP}$ and

273 respective peptidoglycan substrates (C). Overlayed SPR sensorgrams for general binding of substrates
274 to $PcsB_{CHAP}$ (D), summary of kinetic parameters derived from SPR analysis assuming 1:1 binding of
275 $PcsB_{CHAP}$ to various substrates (E). Single asterisks (*) in table E indicate significantly poor fittings as
276 per Biacore Insight analysis software. Error bars denote standard deviation around mean. Significance
277 determined by t-test. n.s. $p>0.05$, ** $p<0.01$, *** $p<0.001$, **** $p<0.0001$
278
279 We used surface plasmon resonance (SPR) with selected commercially available
280 peptidoglycan fragments to interrogate protein-ligand binding interactions further with the
281 $PcsB_{CHAP}$ protein bound to an SPR chip surface. When the bound protein was challenged with
282 the pentapeptide stem peptide alone, amidation (of Glutamate to iso-glutamine) at the
283 second position (A*i*Qk$A_D$$A_D$ appears to induce an approximate 15-fold increase in binding KD
284 compared to the non-amidated (AEKA_DAD) isoform (Fig. 2 E, in which the amidated peptide
285 form corresponds to the species found in *S. pneumoniae* PG (Fig. 2 C). The performance
286 characteristics of the pentapeptide in this experiment are non-ideal, however are consistent
287 with on-chip hydrolysis of the pentapeptide by the $PcsB_{CHAP}$ domain . The dipeptides γ-D-Glu-
288 mDAP (iE-DAP) or γ-D-Glu-Lys (iE-Lys) dissociate with highly similar affinities, so we extended
289 this to include tripeptide species (classical NOD1 and NOD2 ligands (49–51)) that included the
290 N-acetylmuramic acid residue. We therefore used MurNAc-Ala-D-isoGln-Lys (M-TriLYS) and
291 MurNAc-L-Ala-γ-D-Glu-mDAP (M-TriDAP) as ligands in the experiment and recorded slightly
292 improved affinities (KD) compared to the dipeptide (Fig 2 D/E). It should be noted that the
293 presence of the amidation, as well as the sugars in M-TriDAP and M-TriLYS substrates, seems
294 to be required for the enzyme recognition, as sensorgram profiles from the kinetics/affinity
295 analysis of those substrates (Fig. 2E and Supp Fig 5) are consistent with on-chip enzyme
296 activity, given the lower general resonance units (RU), which is proportional to the number of
297 molecules bound to the surface, compared to other substrates, indicating that they are being
298 actively hydrolysed and that the product is not remaining bound to the captured enzyme. The
299 interaction with N-Acetylmuramyl-L-Alanyl-D-Isoglutamine (MDP) gave no data that could be
300 interpreted with our SPR experiment and unfortunately an N-Acetylmuramyl-pentapeptide
301 species is not commercially available. Taken together, this binding analysis suggests that
302 $PcsB_{CHAP}$ substrate binding is dependent on both Lys and *iso*Gln presence, but may be
303 enhanced by the sugar component of the ligand.
304

305 Finally, we determined the PG cleavage site upon which $PcsB_{CHAP}$ acts. Incubation of synthetic
306 pneumococcal stem peptide substrate L-Ala-D-isoGln-L-Lys-D-Ala-D-Ala (A*i*QK$A_D$$A_D$) with
307 $PcsB_{CHAP}$ was initially separated using thin-layer chromatography (TLC) (Supp Fig. 6A), which
308 revealed a polar entity moving with the solvent front to a high position on the TLC plate that
309 did not appear in any other lane. We therefore isolated the fragments of peptide and
310 conducted mass spectrometry (MS) analysis on the products. The m/z peak corresponding to
311 the full pentapeptide (488) was detected (Supp Fig. 6B), which fragmented well under high
312 energy and predictably such that the full pentapeptide could be assigned (Supp Fig. 6C). Two
313 other peaks were also identified at m/z values of 218 and 289 which are consistent with
314 fragments for A*i*Q and K$A_D$$A_D$ originating from A*i*QK$A_D$$A_D$ peptide. High energy fragmentation
315 of the 218 and 289 peaks allowed assignment of both peptide products respectively (Supp
316 Fig. 6D and E), leading to the conclusion that PcsB is an endopeptidase and specifically cleaves
317 the bond between the *iso*Glutaminyl and Lysyl residues at position two and three in the PG
318 stem respectively. This is further confirmed by our binding analysis of the MDP substrate to
319 $PcsB_{CHAP}$ (Fig. 2 D and E) which suggested low-to-no interaction, something expected of the
320 product of the enzymatic cleavage.
321
322 To examine this further, we mutated the PcsB active site Cys292 to Ser in an attempt to trap
323 the reaction intermediate in a more stable oxy-ester form compared to the native thio-ester.
324 Following site-directed mutagenesis of the expression construct and subsequent expression
325 and purification of the $PcsB_{CHAP\ C292S}$ protein, the native pentapeptide substrate (A*i*QK$A_D$$A_D$)
326 was incubated with the protein at an equimolar concentration. Following subsequent SDS-
327 PAGE separation of the protein, an in-gel trypsin digest was carried out prior to mass
328 spectrometry analysis of the peptide products. This revealed a shift in mass of +213 m/z,
329 equivalent to the A*i*Q moiety bound via an ester to the now active-site Ser residue (Supp Fig.
330 6F). This confirms both the scissile bond in this reaction as well as part of the mechanism of
331 action of PcsB.
332
333 Whilst multiple attempts were made to crystalise $PcsB_{CHAP}$ in the presence of substrate(s) or
334 the oxy-ester intermediate, we were only able to capture the apo states of both $PcsB_{CHAP}$
335 (PDB: 9R6W) and $PcsB_{CHAP\ C292A}$ (PDB: 9R7G); (Supp Fig. 7) which showed negligible changes in
336 conformation when compared to the previously published structure indicating that there is

337 no change in the CHAP domain itself responsible for catalytic activation (4). By combining our
338 in vitro activity data with our mass spectrometry data, we propose a mechanism for how the
339 CHAP domain of PcsB catalyses the cleavage of the peptide stem within *S. pneumoniae* PG
340 (Fig. 3).
341

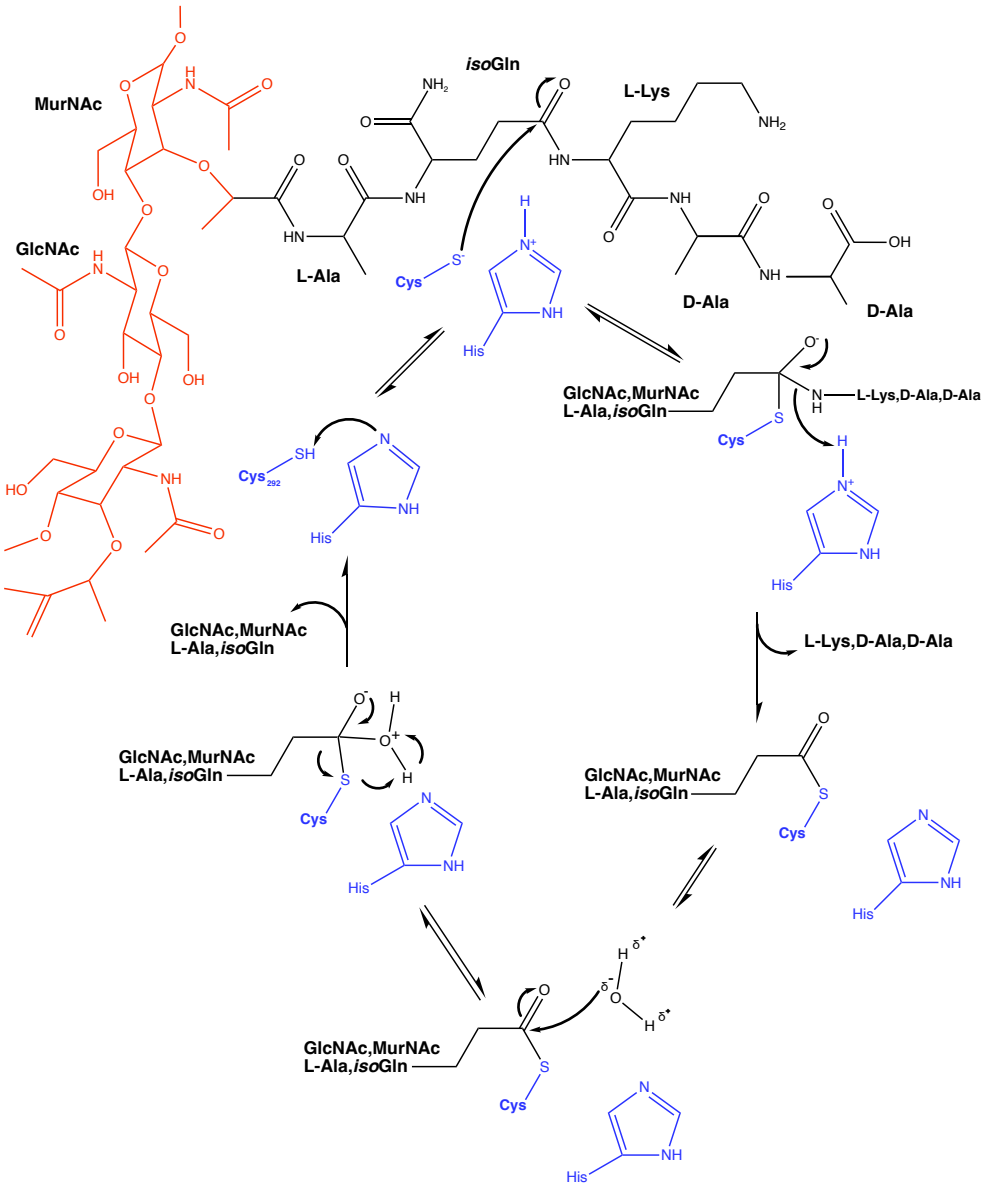

342
343 **Figure 3 - Proposed reaction schematic for PcsB**. Blue moieties denote side chains belonging to
344 PcsB protein structure (Cys_{292}, His_{343}), whilst red denotes the glycan strand and black denotes the
345 pentapeptide side chain. In our proposed mechanism, Cys_{292}, assisted by proton transfer to
346 His_{343}, initiates SN2 nucleophilic attack on the carbon atom of the peptide bond between *iso*Gln
347 at position 2 and lysine at position 3 in the peptidoglycan side chain. The resulting tetrahedral

348 transition state collapses, forming a PcsB-thioester intermediate, with expulsion of Lys-D-Ala-D-
349 Ala, facilitated by protonation of the latter by His_{343}. The thioester between PcsB-Cys292 and the
350 remaining GlcNAc MurNAc L-Ala-*iso*Gln is subsequently hydrolysed via a second tetrahedral
351 transition state (probably via a water nucleophile, consistent with a classical Cys protease
352 mechanism (50)) to generate a carboxylic acid moiety on the Peptidoglycan Ala-*iso*Gln stub and
353 regenerate the free PcsB CHAP domain for subsequent rounds of catalysis.
354
355 Taken together, these results support a hypothesis that PcsB activity is optimised for (but not
356 exclusive to) the pneumococcal PG substrate, rather than other forms of PG found in other
357 bacterial species and that the enzymatic activity of the CHAP domain is consistent with an iso-
358 Glutaminyl-Lysyl DL-endopeptidase, i.e. cutting between the second and third positions in the
359 pentapeptide stem. Whilst PcsB is secreted into the media during pneumococcal growth (4),
360 the lack of activation of the CHAP domain data (Fig. 2 (4)) argues against it having activity
361 against competing bacterial species, however. The ability of the CHAP domain to perform
362 catalysis on a non-cognate substrate including the *E.coli* peptidoglycan is consistent with our
363 previous co-overexpression and rescue complementation experiments of *Spn* FtsEX-PcsB in
364 *E. coli* (Fig. 1 B/C, Supp Fig. 2 I) having phenotypic effects consistent with a role in cell division.
365 Finally, the conservation of structure seen between the CHAP domain in isolation determined
366 here compared to that seen in context of the full-length PcsB structure suggests that DL-
367 endopeptidase activity requires major conformational changes are in the coiled-coil domain,
368 not the CHAP domain..
369
370 **The helix adjacent to PcsB's CHAP domain has a biological function in regulating PcsB**
371 **endopeptidase activity.**
372 In *E. coli*, as well as other Gram-negative bacteria, a pair of Zn^{2+}-dependent amidases
373 (AmiA/B) are known to bind FtsEX-EnvC and denude glycan strands via hydrolysis of the
374 MurNAc-Ala ester bond (52,53). These amidases have also been shown to be regulated via
375 helical structures adjacent to the hydrolytic domain of the proteins (23). Similarly, the *B.*
376 *subtilis* endopeptidase, LytE, is regulated via a flexible loop from IseA that occludes the active
377 site (24). A previous structure of PcsB (4) showed a similar short helix (N256-S267) close to

378 the CHAP domain, proceeded by a flexible loop region (A269-T282). We therefore
379 investigated if this region had a similar regulatory function within the PcsB system.
380
381 The full length *pcsB* gene was truncated to remove the coiled-coil domain, leaving only the
382 11-residue helix of interest, disordered region and CHAP domain referred to thus as $PcsB_{CHAP+}$
383 (residues T255-D392)) (Fig. 4A). This was cloned into and expressed from pET-28b, with the
384 protein subsequently purified by Ni^{2+} IMAC (Supp Fig. 3F). Assessment of this protein's
385 activity using the 206nm light-scattering assay revealed no significant difference in activity
386 from the full-length PcsB protein (Fig. 4B), in contrast to the isolated CHAP domain. This is
387 consistent with a specific role for this helical-disordered region in inhibiting the catalytic
388 activity of the CHAP domain.
389
390 We hypothesised that this helix was being repositioned by the disordered region proceeding
391 it such that the active site of PcsB was occluded. An alternative explanation for this
392 observation is that the purified protein is aggregating via the helix and thus held in an inactive
393 state in solution. We investigated this using size-exclusion chromatography (SEC), which
394 revealed both the $PcsB_{CHAP}$ and $PcsB_{CHAP+}$ proteins migrate as equivalent monodispersed
395 species (Fig. 4C). Neither protein showed evidence of aggregation, from which we suggest
396 that regulation by the helix is most likely to be via direct interaction with the CHAP domain.
397 It should be noted however that $PcsB_{\Delta 255-273}$ is not catalytically active (Fig. 4B), which could
398 suggest the coiled-coil domain inhibits the CHAP domain directly, or at least that the
399 regulation does not involve this helical region.
400
401

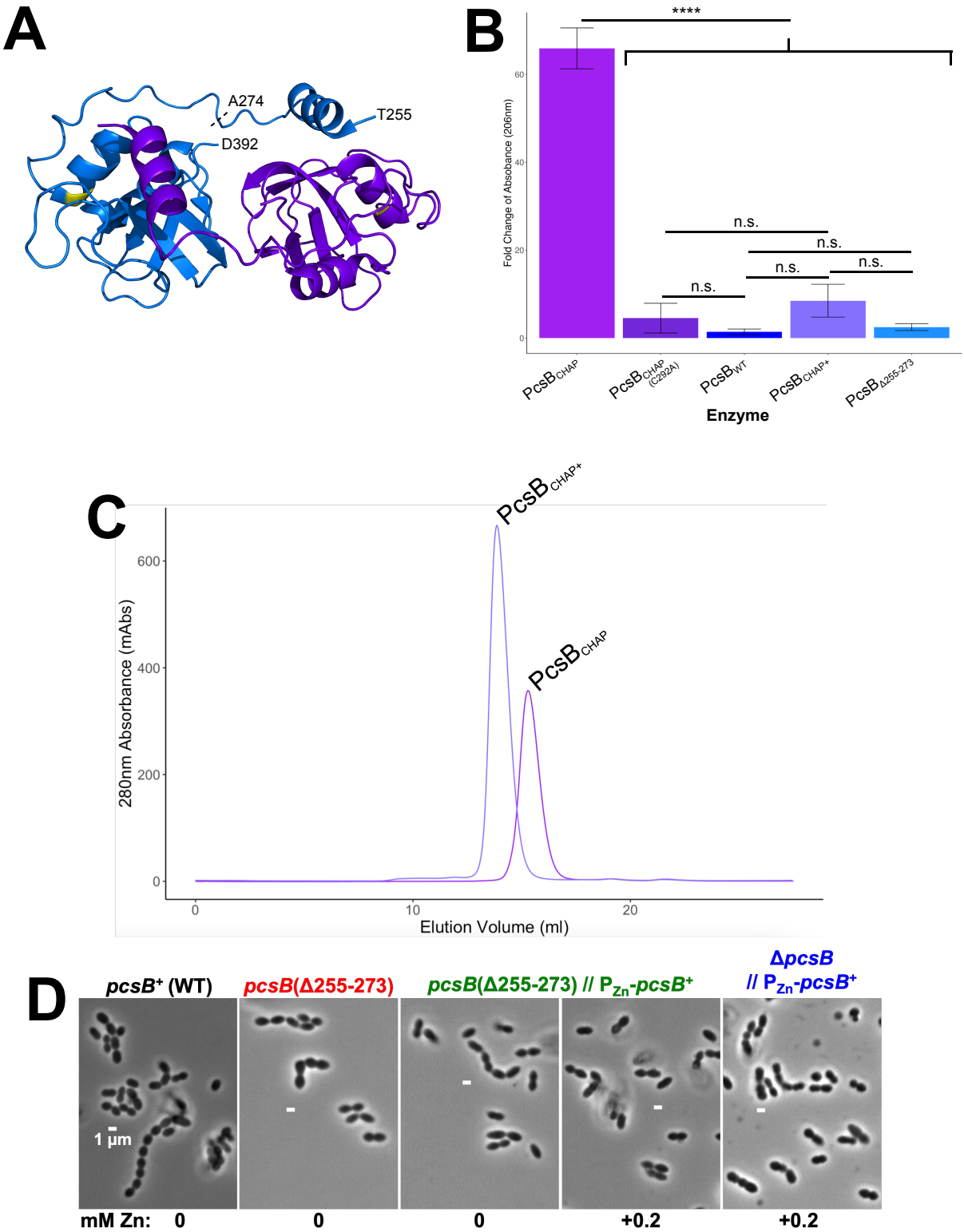

Figure 4 – Short helical region adjacent to CHAP domain of PcsB appears to regulate activity of the PG hydrolase. Visual schematic from published PcsB structure (PDB: 4CGK) indicating CHAP domain with regulatory helix ($PcsB_{CHAP+}$: residues T255-D392). Residue A274 indicates the start of the active endopeptidase CHAP domain, the proposed regulatory helix is shown between T255 and S265 (A). Blue and purple indicate two monomers, active-site Cysteine (C292) shown in yellow. Light scatter-

408 based assay measured at 206nm (B) demonstrating lack of activity of the $PcsB_{CHAP+}$ purified protein.
409 SEC trace of purified $PcsB_{CHAP}$ and $PcsB_{CHAP+}$ proteins (C) indicating migration as a single species with no
410 obvious aggregation. Representative phase contrast micrographs of WT and mutant *Spn* strains (D).
411
412 Since the helix adjacent to PcsB's CHAP domain (amino acids 255-273) largely abolished the
413 *in vitro* endopeptidase activity of $PcsB_{CHAP}$ (Fig. 4B), we asked if this helix regulated PcsB
414 function within the pneumococcus. A pneumococcal mutant lacking this helix, *pcsB*(Δ255-
415 273), expressed PcsB(Δ255-273) at levels comparable to WT (Supp Fig. 8), but showed no
416 growth phenotype in C+Y media (Supp Fig. 9A).
417
418 Mutant *pcsB*(Δ255-273) cells were longer than WT, with increased cell volumes, and
419 complementation with $pcsB^+$ restored cells to WT size (Fig. 4D and Supp Fig 9). This increase
420 in cell size was small but reproducible, and suggests that PcsB endopeptidase activity may be
421 increased in the *pcsB*(Δ255-273) mutant *in vivo*, consistent with the idea that the 255-273
422 helix may partially inhibit PcsB function. However, the *pcsB*(Δ255-273) mutant was not
423 sensitive to antibiotics such as penicillin, fosfomycin, vancomycin, ceftriaxone and
424 cefuroxime, though it was slightly more sensitive to cefotaxime (Supp Fig. 10). Taken
425 together, these results suggest that the 255-273 helix of PcsB has a role in regulating PcsB
426 endopeptidase activity in the pneumococcus, in addition to the ATP hydrolysis action of FtsE,
427 transmitted through FtsX at the membrane and through the coiled-coil region of PcsB to the
428 CHAP domain.
429
430

431 Discussion

432 The role of the FtsEX-PcsB in the context of bacterial cell division has been the subject of
433 increased interest for a number of years. Recent structural elucidation of key components of
434 the wider FtsEX system from multiple organisms has provided some further mechanistic
435 understanding, but a number of key biological questions still remain to be answered. One
436 such question is how is the PG-degrading activity of this protein complex controlled in order
437 to facilitate the required cell division activity? This is especially acute for *S. pneumoniae* since
438 in contrast to many other organisms, the pneumococcal FtsEX-PcsB protein complex is
439 essential for cell survival. Whilst the *E. coli* FtsEX genes are conditionally essential, the growth

440 defect phenotype observed with a Δ*ftsEX* strain under low salt media conditions appears to
441 be rescued by complementation with *Spn* FtsEX alone. Whether this complementation allows
442 recruitment of EnvC-AmiA/AmiB or some other aspect of the protein-protein interactions
443 required for assembly of the *E. coli* divisome is uncertain however. Conversely,
444 overexpression of *Spn* FtsEX induces a filamentous phenotype in *E. coli* that can only be
445 rescued with co-overexpression of the cognate hydrolase *Spn* PcsB, further confirming a
446 functional relationship between these three proteins (1,3,15,16,21). This conclusion is
447 enforced by the examination of mutations in the PcsB and FtsE genes that overexpress
448 nonfunctional PcsB active site cysteine and FtsE ATPase functions respectively at the protein
449 level. This is consistent with a scenario in which the entire *Spn* FtsEX-PcsB system is
450 reconstituted, representing active proteins in both cytoplasmic and extracellular
451 compartments enabling peptidoglycan cleavage. Our detailed mechanistic and structural
452 experiments reinforce this point and provide evidence for endopeptidase activity of PcsB. The
453 ability of the CHAP domain to have low degradative activity toward the non-cognate and
454 chemically distinct *E.coli* peptidoglycan further supports this conclusion.
455
456 This leads to a second question, why is FtsEX widely regarded as being a complex that is
457 recruited early in the assembly of the divisome? The answer to this may lie in part in the
458 elucidation of the enzymatic activities of the hydrolases in question. The *E. coli* AmiA/B are
459 amidases that cleave at the sugar-peptide linkage of the peptidoglycan structure whereas
460 PcsB is an DL-endopeptidase that leaves a dipeptide stub. As recently indicated by work on
461 the SPOR domain of *E. coli* FtsN and its role in binding to denuded glycan and subsequent
462 activation of the FtsWI complex (54), the formation of a modified form of PG may be a crucial
463 marker or stage in the activation of later events in cell division; which in *S. pneumoniae* that
464 may be the sugar-dipeptide stub. Whilst the order of divisome assembly in pneumococcus
465 has not been fully established (but is partly implied from the *E. coli* system (8)), FtsEX-PcsB
466 has been shown to associate with the FtsZ septal ring at midcell of predivisional cells (3,55,56).
467 However as division progresses, FtsX (and by extension FtsE & PcsB) remain at the peripheral
468 (elongasome) synthesis ring, and are therefore separated from the closing septal annulus
469 (56). This localisation pattern previously suggested a role in splitting prior-synthesised septal
470 PG, rather than the daughter cells directly (3,56,57). Given the observation here that PcsB's
471 mechanistic product leaves a sugar-dipeptide stub on the PG, it is possible that a second

472 function of PcsB is to create a signal/space for subsequent PG remodelling to knit together
473 the septal and peripheral rings of PG synthesis post daughter cell separation. It should be
474 noted however that activation of PG synthases during division in pneumococcus is currently
475 not well understood and is an area of active investigation.
476
477 Clearly peptidoglycan needs to be modified to allow cell division but at the same time new
478 material must be synthesised to enable daughter cell separation. These processes are linked
479 but distinctive and intuitively these processes must be highly controlled to prevent
480 inadvertent lysis. The action of the CHAP domain of PcsB in *S. pneumoniae* or AmiA/B in *E.*
481 *coli* will without doubt weaken the peptidoglycan by removing peptide crosslinks between
482 adjacent glycan strands as part of this process. Whilst our focus here has been largely on the
483 role of the extracellular hydrolase, the wider role of FtsEX in protein-protein interactions and
484 assembly has been noted previously including interaction with FtsA (17) and FtsK in *E. coli*
485 (58). It has also been suggested that there is a requirement for interactions between FtsEX
486 and PG synthesis regulators (59), an area that is under current study. However, it should be
487 emphasised that FtsEX-PcsB only associates to septal machinery during early division (7,56)
488 as discussed above. Our phenotypic experiments are consistent with the hypothesis that *Spn*
489 FtsEX interacts with the *E. coli* divisome as described (or at least influences the proper activity
490 of the complex until PcsB co-overexpression induces displacement of the *E. coli* homologs),
491 implying a shared and retained evolutionary history between these bacteria at the level of
492 the divisome. It therefore seems likely that in pneumococcus, FtsEX has a dual role in early
493 divisome recruitment and assembly whilst its ATPase function drives the activation of the
494 extracellular hydrolase activity (to mark the site of division with modified peptidoglycan).
495
496 This subsequently poses the question of the role of PcsB and how it is controlled? We propose
497 on the basis of the evidence presented here and elsewhere that PcsB functions as an essential
498 "space making enzyme" during the cell division process, providing the separation within the
499 sacculus for insertion of nascent glycan strands required for separation at the septal annulus.
500 Tight regulation of PcsB activity is required and this is primarily brought about via
501 conformational change of the coiled-coil region of PcsB as the major regulatory mechanism,
502 resulting from ATP hydrolysis in FtsE transmitted through FtsX. The current hypothesis is that
503 the third helix in the sequence of the PcsB coiled-coil structure extends upwards towards the

504 PG layer thereby allowing the CHAP domain to act at the PG layer. Similar conformational
505 changes have been suggested for homologous systems (5) and as presented in our model (Fig.
506 5). We hypothesise that the short disordered-helical region upstream of the CHAP domain
507 which was noted within the PcsB structure (4) plays an additional role in regulation of the
508 CHAP domain during activation of PcsB by FtsEX, in a similar way to the action of IseA on CwlO
509 in *B. subtilis* (24). Whilst the *in vitro* activity assays suggested that this short region oblates
510 the activity of the CHAP domain completely, *in vivo* deletion of this region did not produce a
511 constitutively activated protein. Instead, the cells showed a significant enlargement to their
512 length and cell volume, implying that the major control mechanism is still through PcsB's
513 interaction with FtsEX, but that this short helix is likely to play a more subtle role in a CHAP-
514 domain-specific manner.
515

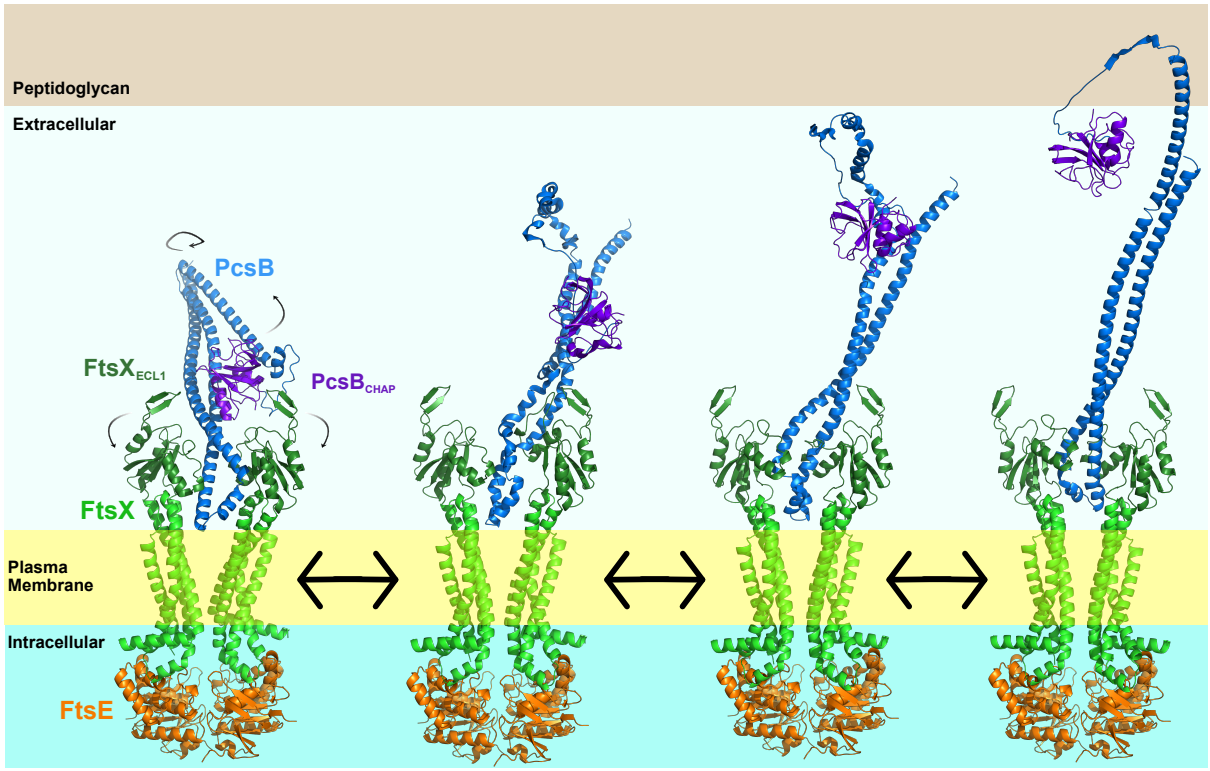

516
517 **Figure 5 - Proposed activation mechanism for PcsB via FtsEX.** Turnover of ATP by FtsE in the
518 cytoplasm induces a conformational change in FtsX imbedded in the cytoplasmic membrane that in
519 turn enables a conformational change in the coiled-coil region of PcsB. Extension of the coiled-coil
520 region of PcsB liberates the CHAP domain from an inactive to an active state, allowing it to act on the
521 peptidoglycan layer as an iso-Glutaminyl-Lysyl DL-Endopeptidase, producing a modified glycan with a
522 dipeptide stub marking the site for further cell division activity. A short helical region adjacent to the

523 CHAP domain provides additional regulation of endopeptidase activity. Models generated using
524 AlphaFold3, intermediate steps generated using Pymol3 Morphing function.
525
526 Finally, we should ask the question of why *Spn* PcsB is essential? Taking the data presented
527 here and elsewhere on balance, we propose that *Spn* PcsB has an essential role in *S.*
528 *pneumoniae*, which classically has been in relation to cell separation (4,60). Here we
529 introduce an additional role to that of septal annulus ring splitting previously proposed
530 (56,57) as the protein appears to produce a modified form of peptidoglycan which marks the
531 area of the cell required for synthesis of new material following division. This activity is
532 controlled by ATPase activity in FtsE inducing mechanochemical confirmational change
533 through FtsX and into PcsB to activate DL-Endopeptidase activity. Additionally, FtsEX makes
534 interactions with other parts of the divisome apparatus early in the cell division process as a
535 coordinating element in the process which appears to be a conserved function across species.
536 Whilst the enzymatic process of marking the site of division is performed by multiple systems
537 in other bacteria including *E. coli* where the FtsEX-EnvC-AmiA/AmiB function can be
538 compensated by multiple redundancies, in *S. pneumoniae* the role of FtsEX and PcsB is to
539 make a MurNac-dipeptide stub within the peptidoglycan layer, marking the site of division;
540 hence why PcsB is essential. In *E. coli* the SPOR domain containing protein FtsN recognises
541 fully denuded PG and orchestrates later events in cell division. *S. pneumoniae* has no SPOR
542 domain proteins and thus a question arises as to what protein or proteins perform that
543 function. The answer to this question is an active part of the research carried out in our
544 laboratories and others.
545
546 In summary, we have demonstrated here that PcsB's activity is specifically that of an
547 *iso*Glutaminyl-Lysyl-endopeptidase which acts against pneumococcal cell wall PG and is
548 predominantly regulated via the coiled-coil region, but also by a short regulatory helix that
549 acts specifically on the CHAP domain. This work provides further insight into the molecular
550 events to activate PcsB via ATP hydrolysis in FtsE, enabling mechanochemical conformational
551 change from inside the cytoplasm via FtsX to PcsB on the extracellular surface and new
552 molecular level detail on the mechanism and chemical features of PG cleavage during
553 pneumococcal cell division. These data may contribute to further exploration of PcsB as an
554 Achilles' heel to target for future selective antimicrobial strategies against pneumococci (3).

555

556 ## Acknowledgements

557 SN was supported by MRC Doctoral Training Partnership grant MR/N014294/1 and a Medical
558 and Life Sciences Research fund award. NB was supported by a Ph.D. studentship to the
559 Midlands Integrative Biosciences Training Partnership BBSRC grant BB/J014532/1 and by the
560 Howard Dalton Centre at the University of Warwick under its small grant scheme award to
561 support this work. SC was supported by MRC Infection and Immunity award MR/Z504245/1.
562 Research in the laboratory of DR is supported by MRC grants MR/Z504245/1 and BBSRC
563 grant BB/Y003187/1 and previously by a sabbatical Schaefer Research Scholars Program
564 Awards to Columbia University NYC. Research in the laboratory of MW is supported by NIH
565 Grant R35GM131767.

566

567 # Materials & Methods

568 **Spot Titre Assay**

569 *E. coli* parent and *ftsEX* knockout strains (Supplementary Table 1) were gifted by Jonathan
570 Cook, (Crow Lab, University of Warwick) and subsequently transformed with pET-DUET1-
571 FtsEX construct containing the pneumococcal *ftsEX* gene cassette (Supplementary Table
572 2). Cells were subsequently cultured in LB (10g/L NaCl) broth with appropriate antibiotic
573 selection up to an OD_{600} of around 1 before being serially diluted in PBS and spot plated onto
574 LB agar or LB0N (0g/L NaCl) agar plates. Plates were incubated at 20°C overnight and imaged
575 using ChemiDoc Imaging system (BioRad).

576

577 *E. coli* Growth and **Microscopy**

578 *E. coli* BL21 $(DE3)_{ftsZ\text{-}mNEON}$ cells were transformed with the construct(s) of interest. For growth
579 curve analysis, cells were diluted to OD_{600} = 0.005 from overnight cultures and added to Cyto-
580 One 96-well plates (StarLabs) in 2YT-AI media with appropriate antibiotics in triplicate. The
581 plate was then incubated at 37°C for 24hrs in a BioTek Cytation 5 plate reader (Agilent). OD_{600}
582 readings were taken every 15mins over this period. Data visualised using ggplot package via
583 R (V2024.04.1+748) For microscopy, overnight cultures were diluted in fresh LB 1:1 before
584 being incubated with 1mg/ml D,L-Serine Hydroxymate for 90 min. Cells were washed in LB
585 before being diluted to OD_{600} = 0.05, and cultured at 37°C with antibiotic selection in 2YT

586 autoinduction media (Formentum Cat#: AIM2YT0210) until OD_{600} = 0.8-1. The temperature
587 was then reduced to 20°C overnight to allow expression of proteins. The following morning,
588 cells were placed onto microscopy slides using a 1% agarose pad and imaged on Leica DMi8
589 Inverted Microscope.
590
591 **Protein Expression and Purification**
592 Constructs were transformed into BL21 (DE3) Star:pRosetta *E. coli* and grown overnight at
593 37°C. Cultures were then diluted into 2YT growth media with appropriate antibiotic selection
594 up to an OD_{600} = 0.4-0.6, at which point IPTG was added to 300 µM. The temperature was
595 reduced to 28°C and induction proceeded for 3 h prior to cell harvest at 6000 x *g*. Cells were
596 then resuspended in 50 mM Tris-HCl (pH 7.5), 500 mM NaCl, 10% Glycerol, 3 mg/L Lysozyme
597 and sonicated to lyse the culture before cell debris was pelleted at 40,000g. The soluble
598 fraction of the cells was then loaded on a FastFlow 5ml HisTrap column (Cytiva) that had been
599 pre-charged with 50mM Tris-HCL (pH 7.5), 500mM NaCl, 10% Glycerol, 10mM
600 Imidazole. Column washing proceeded using 20%, 50% and 100% (50mM Tris-HCL (pH 7.5),
601 500mM NaCl, 10% Glycerol, 500mM Imidazole) solutions, fractions of which were collected
602 and analysed for protein content via SDS-PAGE. Fractions containing purified protein were
603 buffer exchanged into 50mM Tris-HCL (pH7.5), 200mM NaCl, 10% Glycerol, flash frozen and
604 stored at –80°C.
605
606 For PcsB purification from pneumococcal growth media, a *Spn* strain was created expressing
607 PcsB-His6x (strain IU18999). See the "*Streptococcus pneumoniae* Strain Construction"
608 methods section below, as well as Supplementary Table 3, for details. This strain was cultured
609 statically in BHI ± 1% choline chloride overnight at 37 °C + 5% CO_2. Pneumococcal cells were
610 removed by centrifugation at 4000g before the media was loaded onto a FastFlow 5ml
611 HisTrap column (Cytiva) that had been pre-charged with 50mM Tris-HCL (pH 7.5), 500mM
612 NaCl, 10% Glycerol, 10mM Imidazole. Column washing proceeded using Tris-HCL (pH 7.5),
613 500mM NaCl, 10% Glycerol, 50mM Imidazole solution before elution using Tris-HCL (pH 7.5),
614 500mM NaCl, 10% Glycerol, 500mM Imidazole solution. Fractions containing purified protein
615 were buffer exchanged into 50mM Tris-HCL (pH7.5), 200mM NaCl, 10% Glycerol, flash frozen
616 and stored at –80°C.
617

618 **Light-Scattering Peptidoglycan Degradation Assay**

619 Cell wall PG was purified from overnight cultures grown on respective agar plates (*E. coli* – LB,
620 *S. pneumoniae* – BHI (+5% defibrinated horse blood), *M. leutus* and *M. smegatis* –
621 Nutrient). Cells were collected via cotton swabs into vials containing 1M NaCl prior to being
622 boiled for 1hr. Following centrifugation, and washing with sterile water, a DNase/RNase
623 solution was added (15µg/ml and 60µg/ml respectively) and allowed to incubate. Further
624 boiling the suspension(s) preceded centrifugation and sterile water washing before the final
625 suspension as made up in 12.5mM $NaPO_4$ (pH 5.3). This cell wall was then added to a UV-vis
626 quartz cuvette to a final concentration of 0.04% in 25mM KPO_4. Once a stable baseline was
627 established using a Cary-200 Spectrophotometer, protein was added to a final concentration
628 of 286µM and the initial rate recorded.

629

630 **Thin Layer Chromatography**

631 Purified $PcsB_{CHAP}$ was mixed with the synthetic pentapeptide A*i*QK$A_D$$A_D$ (Sigma) at a 1:5 molar
632 ratio (69.2µM and 346µM respectively) and incubated at 37°C overnight. Samples were
633 separated on aluminium plated silica-60 TLC plates (Fisher) and spots dried before being
634 separated using the mobile phase 3:1:1 n-butanol:acetic acid:water. Bands were visualised
635 using ninhydrin stain.

636

637 **Mass Spectrometry**

638 $PcsB_{CHAP}$ protein was incubated with synthetic pentapeptide A*i*QK$A_D$$A_D$ at a 1:5 protein:ligand
639 molar equivalence overnight at 37°C. Protein was removed by centrifugal filtration using a
640 3kDa cut-off filter, allowing the peptide fragments to pass through. These were collected and
641 analysed by direct spray ionisation mass spectroscopy in collaboration with Cleidiane
642 Zampronio at WPH Proteomics Facility (University of Warwick). Samples were digested with
643 Trypsin as per established protocols of the facility before being electrosprayed directly (~300
644 nL min-1) through a Triversa Nanomate nanospray source (Advion Biosciences, NY) into a
645 Thermo Orbitrap Fusion mass spectrometer (Q-OT-qIT, ThermoFisher Scientific, Germany) in
646 positive ion mode. The gas flow was set to 0.3 psi and the voltage 1.7 kV. Data were acquired
647 from 150 to 500 m/z with 120 K resolution (at 200 m/z). The precursor ions 218m/z, 289 m/z
648 and 488 m/z were isolated and submitted to HCD fragmentation and detected on the
649 Orbitrap. MS/MS analysis was performed using collision energy 35.

650

651 **Surface Plasmon Resonance**

652 Kinetic parameters for the interaction of $PcsB_{CHAP}$ with $AEKA_DA_D$, A*i*QKA_DA_D (Sigma), MDP, iE-
653 LYS, iE-DAP, M-TriDAP & M-TriLYS (Invitrogen) were measured by multicycle Surface Plasmon
654 Resonance (SPR) on a Biacore T200 (GE Healthcare) employing a NTA Series S sensor chip
655 (Cytiva). Prior to the analysis, the chip was conditioned with 350 mM EDTA and activated at
656 the start of each cycle with 0.5 mM $NiCl_2$. Chip regeneration at the end of each cycle was
657 achieved with 30 s injection of 350 mM EDTA. His-tagged $PcsB_{CHAP}$ (ligand) was buffer
658 exchanged into running buffer (0.22 µm filtered PBS + 1% DMSO) using Zeba Spin desalting
659 columns (Thermo Fisher Scientific) and diluted to a final concentration of 100 nM. PG
660 fragments used as analytes were resuspended in running buffer to a final concentration of 10
661 mg/ml and eventually diluted to the starting concentration of 125 µM. Upon ligand capture,
662 the analytes were injected in decreasing concentrations, following a 1:2 serial dilution from
663 125 µM to 7.812 µM. An injection of 0 µM analyte was employed to be used as blank during
664 kinetics fitting. Contact time for the interaction was kept at 120 s, and the complex was left
665 to dissociate by injecting running buffer for 600 s prior to regeneration. The same overall
666 procedure was used to obtain a sensorgram overlay of the general binding between the
667 analytes and $PcsB_{CHAP}$. In this method, 100 µM analyte was injected for 60 s onto the captured
668 protein and let dissociate for 60 s.

669

670 Data analysis was performed on the Biacore Insight Evaluation software. Sensorgrams from
671 the general binding method were overlayed and normalized after the capture level was
672 assessed to counter the baseline shifting of the captured ligand and to allow an easier
673 amplitude measurement. Kinetic parameters (k_a = association constant, k_d = dissociation
674 constant, R_{max} = maximum response signal, KD = equilibration dissociation were obtained by
675 employing a 1:1 Langmuir interaction fitting model to calculate the KD.

676

677 **Protein Crystallisation and Structural Determination**

678 Proteins were purified as described above and concentrated to 8-10mg/ml. Simultaneously,
679 80 µL of each sparce-screen condition (Structure-screen, JCSG+, Morpheus, MIDAS or ProPlex
680 from Molecular Dimensions) was added to the reservoir of an MRC 2-drop plate
681 (SWISSCI). Using the Formulatrix NT8 robot, protein samples were mixed with each reservoir

682 condition at either 1:1 or 1:2 (protein:condition) ratio by volume before being covered with
683 an optically clear sealing sheet (Molecular Dimensions) and incubated at 18°C. Each drop was
684 checked daily for the first 7 days, then once a week afterwards under an SZX16 microscope
685 (Olympus).
686
687 Identified crystals ($PcsB_{CHAP}$ grown in 100mM Sodium citrate(pH 5.6), 500mM NaCl, 4 % v/v
688 Polyethyleneimine (Molecular Dimensions Structure Screen condi8on G7; $PcsB_{CHAP\ C292A}$
689 grown in 100mM BICINE (pH 9), 10% w/v PEG 6000 (Molecular Dimensions JCSG+ conditon
690 E10)) were loop fished into 25% ethylene glycol (made up in crystallisation condition) and
691 flash frozen in liquid nitrogen for transport to Diamond Light Source in Uni-Pucks (Jena
692 Bioscience). Data was collected on the i04 beamline, with a total of 3600 images taken across
693 360° of rotation and auto-processed using the xia3 pipeline before being re-processed using
694 Aimless (61) to removed batches that correspond to crystal degradation. Following
695 determination of monomer number using Matthews (62), and generation of molecular
696 replacement template using Swiss-model (63–65), PhaserMR was used to generate a solution
697 structure based on the diffraction data that could then be refined using Coot (66–68) &
698 Refmac5 (69). Model quality was checked using in-built validation tools within Coot as well
699 as the B-average programme (66–68).
700
701 **Size Exclusion Chromatography**
702 Purified proteins were injected onto a Superdex 75 10/300 GL via an AKTA Pure system which
703 had previously been washed with 1 column volume (CV) water and 1 CV 25mM Tris-HCL (pH
704 7.5), 200mM NaCl at appropriate flow rates. Flow was carried out against gravity and
705 separation monitored at 280nm. Fractions were collected using an F9-C automated fractions
706 collector prior to peak fractions being analysed via SDS-PAGE.
707
708 ***Streptococcus pneumoniae* Strain Construction**
709 *Streptococcus pneumoniae* strains used in this study were derivates of serotype 2 strain D39W
710 (70) and are listed in Supplementary Table 3. *Spn* genomic DNA and oligonucleotides listed in
711 Supplementary Table 4 were used to perform overlapping fusion PCR and generate linear
712 amplicons. For transformation, *Spn* cells grown in brain heart infusion broth (BHI, BD Bacto
713 237500) at 37°C (all *Spn* incubations were done in a 5% CO_2 atmosphere without shaking) to

714 an OD_{620} ≈0.030 were diluted 1:10 in BHI broth containing 10% (v/v) heat-treated horse
715 serum, 10 mM glucose and 100 ng/mL synthetic competence-stimulating peptide 1 (CSP-1)
716 (71). Cells were incubated at 37°C for 10 m to induce competence before addition of 30-100
717 ng amplicon DNA, then incubated an additional 1 h. 100-800 µL cells were then added to 3
718 mL melted NB soft agar (0.8% (w/v) Nutrient Broth (BD Difco, 234000) and 0.7% (w/v) Agar
719 (BD Bacto, 214010)) containing selective antibiotics and plated on trypticase soy agar
720 containing 5% (v/v) defibrinated sheep blood (TSA-BA, BD BBL, 221261) and incubated
721 overnight at 37°C. Single colonies were isolated on two successive days to fresh TSA-BA plates
722 with selective antibiotics and incubated overnight at 37°C. For storage, a single colony was
723 grown at 37°C in 3 mL BHI broth with selective antibiotics to OD_{620} 0.1-0.15, mixed with
724 glycerol (final 15% (v/v)) and stored at -80°C. For antibiotic selection, 0.3 µg/mL erythromycin,
725 250 µg/mL streptomycin and 250 µg/mL kanamycin was used. Where necessary, cells were
726 supplemented throughout transformation, plating, single-colony isolation and storage with
727 0.4 mM $ZnCl_2$/0.04 mM $MnSO_4$ (Zn with one-tenth concentration Mn included to prevent Zn
728 toxicity, referred to elsewhere as "Zn inducer") to induce gene expression at the ectopic *bgaA*
729 locus through a zinc-inducible promoter (72).
730
731 ***Spn* Growth and Microscopy**
732 To make overnight cultures, frozen glycerol stocks were inoculated into 4 mL BHI broth,
733 serially diluted and incubated 12-16 h at 37°C. When needed, overnight cultures were
734 supplemented with 0.4 mM Zn inducer. For growth curve analysis in BHI broth, overnight
735 cultures in exponential phase (OD_{620} 0.1-0.4) were diluted to OD_{620} 0.003 in 6 mL fresh BHI
736 broth with or without 4 µM ComS* (73). Cultures were incubated at 37°C, and the OD_{620} was
737 monitored every 45 m. For growth curve analysis in C+Y media (74,75), 2 mL overnight cell
738 culture in exponential phase were centrifuged at 21,100 x *g* for 5 m at room temperature (RT),
739 washed in 1 mL C+Y media, centrifuged again, and resuspended in 4 mL fresh C+Y. Cultures
740 were diluted to OD_{620} 0.003 in 5 mL fresh C+Y with or without 0.2 mM Zn inducer, incubated
741 at 37°C, and OD_{620} monitored every 45 m.
742 For microscopy, 500 µL cultures at OD_{620} 0.1-0.15 were centrifuged at 21,100 x *g* for 3 m at
743 RT. 470 µL of the supernatant was removed and the pellet was resuspended in the remaining
744 liquid with gentle pipetting. 1.25 µL of resuspension was placed on a glass microscope slide
745 and a glass coverslip was gently applied. A Nikon Eclipse E-400 microscope, Nikon NIS-

746 Elements BR imaging software, and a Nikon DS-Qi2 camera were used to capture phase-
747 contrast images with 20-50 ms exposure time. Lengths and widths of >100 cells from 2
748 biological replicates were measured using Nikon NIS-Elements BR imaging software, and
749 dimension parameters were compared between strains using a Kruskal-Wallis test with
750 Dunn's multiple comparisons test (GraphPad Prism v10).
751
752 ***Spn* Disc Diffusion Antibiotic Sensitivity Assay**
753 Performed as described previously (76), with slight modifications. Briefly, frozen glycerol
754 stocks were inoculated in 3 mL BHI broth and incubated at 37°C. When OD_{620} reached 0.1-
755 0.15, cultures were diluted to OD_{620} 0.009 in fresh BHI broth. 50 µL of cells were added to 3
756 mL melted NB soft agar, poured onto TSA-BA plates and incubated for 15 m at RT to solidify.
757 After incubation, a paper disc containing an antibiotic (BD Sensi-Disc™, Penicillin 230918,
758 Cefotaxime 231606, Tetracycline 230998, Fosfomycin 231709, Vancomycin 231034,
759 Ceftriaxone 231634, Chloramphenicol 230733, Cefuroxime 231621) was placed in the center
760 of each plate, and plates were incubated at 37°C. After 16 h, the diameter of the zone of
761 inhibition was measured. Measurements were averaged from 3 biological replicates and
762 compared to WT using an unpaired *t* test (GraphPad Prism).
763
764 ***Spn* Quantitative Western Blotting**
765 Quantitative western blotting of *Spn* cell lysates was performed as described previously for
766 anti-aPBP1a and anti-MpgA antibodies (77), with minor modifications. Briefly, overnight
767 cultures were supplemented with 0.4 mM Zn inducer as needed, and overnight cultures in
768 exponential phase were washed and resuspended as described previously and diluted to
769 OD_{620} 0.003 in 5 mL fresh C+Y with or without 0.2 mM Zn inducer as needed. Cell growth, cell
770 lysis, SDS-PAGE, transfer to nitrocellulose, total protein stain and blocking were carried out as
771 described previously. The primary antibody used was a rabbit anti-PcsB antibody (1:1,000
772 dilution), generated by ThermoFisher Scientific using full-length *Streptococcus pneumoniae*
773 D39 PcsB (amino acid M1 to D392, with an additional N-terminal sequence of LEHHHHHH)
774 expressed in *E. coli* and purified as described above. Secondary antibody blotting, washing,
775 imaging and quantitation of protein amount was completed as described previously (77).
776 Shown is a representative result from 2 biological replicates.
777

Bibliography

1. Sham LT, Jensen KR, Bruce KE, Winkler ME. Involvement of FtsE ATPase and FtsX Extracellular Loops 1 and 2 in FtsEX-PcsB Complex Function in Cell Division of Streptococcus pneumoniae D39. mBio. 2013 Jul 16;4(4):10.1128/mbio.00431-13.

2. Alcorlo M, Straume D, Lutkenhaus J, Håvarstein LS, Hermoso JA. Structural Characterization of the Essential Cell Division Protein FtsE and Its Interaction with FtsX in Streptococcus pneumoniae. mBio. 2020 Sep;11(5):10.1128/mbio.01488-20.

3. Sham LT, Barendt SM, Kopecky KE, Winkler ME. Essential PcsB putative peptidoglycan hydrolase interacts with the essential FtsXSpn cell division protein in Streptococcus pneumoniae D39. Proc Natl Acad Sci. 2011 Nov 8;108(45):E1061–9.

4. Bartual SG, Straume D, Stamsås GA, Muñoz IG, Alfonso C, Martínez-Ripoll M, et al. Structural basis of PcsB-mediated cell separation in Streptococcus pneumoniae. Nat Commun. 2014 May 8;5(1):3842.

5. Chen Y, Guo D, Wang X, Zhang C, Chen Y, Luo Q, et al. Structural insights into the mechanotransducing mechanism of FtsEX in cell division. MedComm. 2024;5(11):e688.

6. Boersma MJ, Kuru E, Rittichier JT, VanNieuwenhze MS, Brun YV, Winkler ME. Minimal Peptidoglycan (PG) Turnover in Wild-Type and PG Hydrolase and Cell Division Mutants of Streptococcus pneumoniae D39 Growing Planktonically and in Host-Relevant Biofilms. J Bacteriol. 2015 Sep 29;197(21):3472–85.

7. Briggs NS, Bruce KE, Naskar S, Winkler ME, Roper DI. The Pneumococcal Divisome: Dynamic Control of Streptococcus pneumoniae Cell Division. Front Microbiol [Internet]. 2021 Oct 18 [cited 2024 Sep 10];12. Available from: https://www.frontiersin.org/journals/microbiology/articles/10.3389/fmicb.2021.737396/full

8. Adams DW, Errington J. Bacterial cell division: assembly, maintenance and disassembly of the Z ring. Nat Rev Microbiol. 2009 Sep;7(9):642–53.

9. Dai K, Xu Y, Lutkenhaus J. Topological characterization of the essential Escherichia coli cell division protein FtsN. J Bacteriol. 1996 Mar;178(5):1328–34.

10. Cell Cycle Machinery in Bacillus subtilis | SpringerLink [Internet]. [cited 2025 Feb 18]. Available from: https://link.springer.com/chapter/10.1007/978-3-319-53047-5_3

11. Barák I, Muchová K, Wilkinson AJ, O'Toole PJ, Pavlendová N. Lipid spirals in Bacillus subtilis and their role in cell division. Mol Microbiol. 2008;68(5):1315–27.

12. Rowland SL, Katis VL, Partridge SR, Wake RG. DivIB, FtsZ and cell division in. Mol Microbiol. 1997;23(2):295–302.

13. Krupka M, Margolin W. Unite to divide: Oligomerization of tubulin and actin homologs regulates initiation of bacterial cell division. F1000Research. 2018 Feb 28;7:235.

14. Egan AJF, Vollmer W. The physiology of bacterial cell division. Ann N Y Acad Sci. 2013;1277(1):8–28.

15. Hao A, Suo Y, Lee SY. Structural insights into the FtsEX-EnvC complex regulation on septal peptidoglycan hydrolysis in Vibrio cholerae. Structure. 2024 Feb 1;32(2):188-199.e5.

16. Li J, Xu X, Shi J, Hermoso JA, Sham LT, Luo M. Regulation of the cell division hydrolase RipC by the FtsEX system in Mycobacterium tuberculosis. Nat Commun. 2023 Dec 4;14(1):7999.

17. Du S, Henke W, Pichoff S, Lutkenhaus J. How FtsEX localizes to the Z ring and interacts with FtsA to regulate cell division. Mol Microbiol. 2019;112(3):881–95.

18. Corbin BD, Wang Y, Beuria TK, Margolin W. Interaction between Cell Division Proteins FtsE and FtsZ. J Bacteriol. 2007 Apr 15;189(8):3026–35.

19. Yang DC, Peters NT, Parzych KR, Uehara T, Markovski M, Bernhardt TG. An ATP-binding cassette transporter-like complex governs cell-wall hydrolysis at the bacterial cytokinetic ring. Proc Natl Acad Sci. 2011 Nov 8;108(45):E1052–60.

20. Pichoff S, Du S, Lutkenhaus J. Roles of FtsEX in cell division. Res Microbiol. 2019 Nov 1;170(8):374–80.

21. Meisner J, Montero Llopis P, Sham LT, Garner E, Bernhardt TG, Rudner DZ. FtsEX is required for CwlO peptidoglycan hydrolase activity during cell wall elongation in Bacillus subtilis. Mol Microbiol. 2013;89(6):1069–83.

22. Cook J, Baverstock TC, McAndrew MBL, Stansfeld PJ, Roper DI, Crow A. Insights into bacterial cell division from a structure of EnvC bound to the FtsX periplasmic domain. Proc Natl Acad Sci. 2020 Nov 10;117(45):28355–65.

23. Cook J, Baverstock TC, McAndrew MBL, Roper DI, Stansfeld PJ, Crow A. Activator-induced conformational changes regulate division-associated peptidoglycan amidases. Proc Natl Acad Sci. 2023 Jun 13;120(24):e2302580120.

24. Tandukar S, Kwon E, Kim DY. Structural analysis of the peptidoglycan DL-endopeptidase CwlO complexed with its inhibitory protein IseA. FEBS J. 2024;291(16):3723–36.

25. Uehara T, Parzych KR, Dinh T, Bernhardt TG. Daughter cell separation is controlled by cytokinetic ring-activated cell wall hydrolysis. EMBO J. 2010 Apr 21;29(8):1412–22.

26. Xu X, Li J, Chua WZ, Pages MA, Shi J, Hermoso JA, et al. Mechanistic insights into the regulation of cell wall hydrolysis by FtsEX and EnvC at the bacterial division site. Proc Natl Acad Sci. 2023 May 23;120(21):e2301897120.

27. Alcorlo M, Martínez-Caballero S, Li J, Sham LT, Luo M, Hermoso JA. Modulation of the lytic apparatus by the FtsEX complex within the bacterial division machinery. FEBS Lett. 2024;598(23):2836–51.

849 28. Pascale GD, Lloyd AJ, Schouten JA, Gilbey AM, Roper DI, Dowson CG, et al. Kinetic
850 Characterization of Lipid II-Ala:Alanyl-tRNA Ligase (MurN) from Streptococcus
851 pneumoniae using Semisynthetic Aminoacyl-lipid II Substrates *. J Biol Chem. 2008 Dec
852 12;283(50):34571–9.

853 29. York A, Lloyd AJ, Genio CI del, Shearer J, Hinxman KJ, Fritz K, et al. Structure-based
854 modeling and dynamics of MurM, a Streptococcus pneumoniae penicillin resistance
855 determinant present at the cytoplasmic membrane. Structure. 2021 Jul 1;29(7):731-
856 742.e6.

857 30. Aggarwal SD, Lloyd AJ, Yerneni SS, Narciso AR, Shepherd J, Roper DI, et al. A molecular
858 link between cell wall biosynthesis, translation fidelity, and stringent response in
859 Streptococcus pneumoniae. Proc Natl Acad Sci. 2021 Apr 6;118(14):e2018089118.

860 31. Filipe SR, Severina E, Tomasz A. The murMN operon: a functional link between antibiotic
861 resistance and antibiotic tolerance in Streptococcuspneumoniae. Proc Natl Acad Sci U S
862 A. 2002 Feb 5;99(3):1550–5.

863 32. Miguel-Ruano V, Acebrón I, Lee M, Martín-Galiano AJ, Freton C, de José UP, et al.
864 Characterization of VldE (Spr1875), a Pneumococcal Two-State l,d-Endopeptidase with a
865 Four-Zinc Cluster in the Active Site. ACS Catal. 2024 Dec 20;14(24):18786–98.

866 33. Ng WL, Robertson GT, Kazmierczak KM, Zhao J, Gilmour R, Winkler ME. Constitutive
867 expression of PcsB suppresses the requirement for the essential VicR (YycF) response
868 regulator in Streptococcus pneumoniae R6. Mol Microbiol. 2003;50(5):1647–63.

869 34. Ng WL, Tsui HCT, Winkler ME. Regulation of the pspA Virulence Factor and Essential pcsB
870 Murein Biosynthetic Genes by the Phosphorylated VicR (YycF) Response Regulator in
871 Streptococcus pneumoniae. J Bacteriol. 2005 Nov;187(21):7444–59.

872 35. Mellroth P, Daniels R, Eberhardt A, Rönnlund D, Blom H, Widengren J, et al. LytA, major
873 autolysin of Streptococcus pneumoniae, requires access to nascent peptidoglycan. J Biol
874 Chem. 2012 Mar 30;287(14):11018–29.

875 36. Arends SJR, Kustusch RJ, Weiss DS. ATP-Binding Site Lesions in FtsE Impair Cell Division. J
876 Bacteriol. 2009 Jun 15;191(12):3772–84.

877 37. Schmidt KL, Peterson ND, Kustusch RJ, Wissel MC, Graham B, Phillips GJ, et al. A
878 Predicted ABC Transporter, FtsEX, Is Needed for Cell Division in Escherichia coli. J
879 Bacteriol. 2004 Feb;186(3):785–93.

880 38. De Leeuw E, Graham B, Phillips GJ, Ten Hagen-Jongman CM, Oudega B, Luirink J.
881 Molecular characterization of Escherichia coli FtsE and FtsX. Mol Microbiol.
882 1999;31(3):983–93.

883 39. Tosa T, Pizer LI. Effect of Serine Hydroxamate on the Growth of Escherichia coli. J
884 Bacteriol. 1971 Jun;106(3):966–71.

885 40. Gubellini F, Verdon G, Karpowich NK, Luff JD, Boël G, Gauthier N, et al. Physiological
886 Response to Membrane Protein Overexpression in E. coli*. Mol Cell Proteomics
887 [Internet]. 2011 Oct 1 [cited 2024 Sep 10];10(10). Available from:
888 https://www.mcponline.org/article/S1535-9476(20)30122-5/abstract

889 41. Wagner S, Baars L, Ytterberg AJ, Klussmeier A, Wagner CS, Nord O, et al. Consequences
890 of Membrane Protein Overexpression in Escherichia coli*. Mol Cell Proteomics. 2007 Sep
891 1;6(9):1527–50.

892 42. Ferullo DJ, Cooper DL, Moore HR, Lovett ST. Cell cycle synchronization of Escherichia coli
893 using the stringent response, with fluorescence labeling assays for DNA content and
894 replication. Methods San Diego Calif. 2009 May;48(1):8–13.

895 43. Schaub R, Dillard J. Digestion of Peptidoglycan and Analysis of Soluble Fragments. BIO-
896 Protoc [Internet]. 2017 [cited 2024 Sep 10];7(15). Available from: https://bio-
897 protocol.org/e2438

898 44. Ferraboschi P, Ciceri S, Grisenti P. Applications of Lysozyme, an Innate Immune Defense
899 Factor, as an Alternative Antibiotic. Antibiotics. 2021 Dec;10(12):1534.

900 45. Höltje JV. Bacterial lysozymes. EXS. 1996 Jan 1;75:65–74.

901 46. Maitra A, Nukala S, Dickman R, Martin LT, Munshi T, Gupta A, et al. Characterization of
902 the MurT/GatD complex in Mycobacterium tuberculosis towards validating a novel anti-
903 tubercular drug target. JAC-Antimicrob Resist. 2021 Mar 1;3(1):dlab028.

904 47. Morlot C, Straume D, Peters K, Hegnar OA, Simon N, Villard AM, et al. Structure of the
905 essential peptidoglycan amidotransferase MurT/GatD complex from Streptococcus
906 pneumoniae. Nat Commun. 2018 Aug 9;9(1):3180.

907 48. Petit JF, Adam A, Wietzerbin-Falszpan J, Lederer E, Ghuysen JM. Chemical structure of
908 the cell wall of Mycobacterium smegmatis. I. Isolation and partial characterization of the
909 peptidoglycan. Biochem Biophys Res Commun. 1969 May 22;35(4):478–85.

910 49. Host Recognition of Bacterial Muramyl Dipeptide Mediated through NOD2:
911 IMPLICATIONS FOR CROHN'S DISEASE. J Biol Chem. 2003 Feb 21;278(8):5509–12.

912 50. Fernandez EM, Valenti V, Rockel C, et al. Anti-inflammatory capacity of selected
913 lactobacilli in experimental colitis is driven by NOD2-mediated recognition of a specific
914 peptidoglycan-derived muropeptide. Gut. 2011;60:1050–9.

915 51. Chamaillard, M., Hashimoto, M., Horie, Y. et al. An essential role for NOD1 in host
916 recognition of bacterial peptidoglycan containing diaminopimelic acid. Nat Immunol.
917 2003;4:702–7.

918 52. van Heijenoort J. Peptidoglycan Hydrolases of Escherichia coli. Microbiol Mol Biol Rev.
919 2011 Nov 29;75(4):636–63.

920 53. Vollmer W, Joris B, Charlier P, Foster S. Bacterial peptidoglycan (murein) hydrolases.
921 FEMS Microbiol Rev. 2008 Mar 1;32(2):259–86.

54. Lyu Z, Yang X, Yahashiri A, Ha S, McCausland JW, Chen X, et al. E. coli FtsN coordinates synthesis and degradation of septal peptidoglycan by partitioning between a synthesis track and a denuded glycan track [Internet]. bioRxiv; 2024 [cited 2025 Mar 10]. p. 2024.05.13.594014. Available from: https://www.biorxiv.org/content/10.1101/2024.05.13.594014v3

55. Perez AJ, Villicana JB, Tsui HCT, Danforth ML, Benedet M, Massidda O, et al. FtsZ-Ring Regulation and Cell Division Are Mediated by Essential EzrA and Accessory Proteins ZapA and ZapJ in Streptococcus pneumoniae. Front Microbiol [Internet]. 2021 Dec 2 [cited 2024 Sep 10];12. Available from: https://www.frontiersin.org/journals/microbiology/articles/10.3389/fmicb.2021.780864/full

56. Perez AJ, Boersma MJ, Bruce KE, Lamanna MM, Shaw SL, Tsui HCT, et al. Organization of peptidoglycan synthesis in nodes and separate rings at different stages of cell division of Streptococcus pneumoniae. Mol Microbiol. 2021;115(6):1152–69.

57. Trouve J, Zapun A, Arthaud C, Durmort C, Guilmi AMD, Söderström B, et al. Nanoscale dynamics of peptidoglycan assembly during the cell cycle of Streptococcus pneumoniae. Curr Biol. 2021 Jul 12;31(13):2844-2856.e6.

58. Pichoff S, Du S, Lutkenhaus J. Disruption of divisome assembly rescued by FtsN-FtsA interaction in Escherichia coli. Proc Natl Acad Sci U S A. 2018 Jul 17;115(29):E6855–62.

59. Brunet YR, Wang X, Rudner DZ. SweC and SweD are essential co-factors of the FtsEX-CwlO cell wall hydrolase complex in Bacillus subtilis. PLOS Genet. 2019 Aug 22;15(8):e1008296.

60. Ng WL, Kazmierczak KM, Winkler ME. Defective cell wall synthesis in Streptococcus pneumoniae R6 depleted for the essential PcsB putative murein hydrolase or the VicR (YycF) response regulator. Mol Microbiol. 2004;53(4):1161–75.

61. Evans PR, Murshudov GN. How good are my data and what is the resolution? Acta Crystallogr D Biol Crystallogr. 2013 Jul 1;69(7):1204–14.

62. Matthews BW. Solvent content of protein crystals. J Mol Biol. 1968 Apr 28;33(2):491–7.

63. Bienert S, Waterhouse A, de Beer TAP, Tauriello G, Studer G, Bordoli L, et al. The SWISS-MODEL Repository—new features and functionality. Nucleic Acids Res. 2017 Jan 4;45(D1):D313–9.

64. Kiefer F, Arnold K, Künzli M, Bordoli L, Schwede T. The SWISS-MODEL Repository and associated resources. Nucleic Acids Res. 2009 Jan 1;37(suppl_1):D387–92.

65. Schwede T, Kopp J, Guex N, Peitsch MC. SWISS-MODEL: an automated protein homology-modeling server. Nucleic Acids Res. 2003 Jul 1;31(13):3381–5.

957 66. Casañal A, Lohkamp B, Emsley P. Current developments in Coot for macromolecular
958 model building of Electron Cryo-microscopy and Crystallographic Data. Protein Sci.
959 2020;29(4):1055–64.

960 67. Emsley P, Cowtan K. Coot: model-building tools for molecular graphics. Acta Crystallogr D
961 Biol Crystallogr. 2004 Dec 1;60(12):2126–32.

962 68. Emsley P, Lohkamp B, Scott WG, Cowtan K. Features and development of *Coot*. Acta
963 Crystallogr D Biol Crystallogr. 2010 Apr 1;66(4):486–501.

964 69. Murshudov GN, Skubák P, Lebedev AA, Pannu NS, Steiner RA, Nicholls RA, et al. *REFMAC*
965 5 for the refinement of macromolecular crystal structures. Acta Crystallogr D Biol
966 Crystallogr. 2011 Apr 1;67(4):355–67.

967 70. Lanie JA, Ng WL, Kazmierczak KM, Andrzejewski TM, Davidsen TM, Wayne KJ, et al.
968 Genome Sequence of Avery's Virulent Serotype 2 Strain D39 of Streptococcus
969 pneumoniae and Comparison with That of Unencapsulated Laboratory Strain R6. J
970 Bacteriol. 2007 Jan;189(1):38–51.

971 71. Håvarstein LS, Coomaraswamy G, Morrison DA. An unmodified heptadecapeptide
972 pheromone induces competence for genetic transformation in Streptococcus
973 pneumoniae. Proc Natl Acad Sci. 1995 Nov 21;92(24):11140–4.

974 72. Eberhardt A, Wu LJ, Errington J, Vollmer W, Veening JW. Cellular localization of choline-
975 utilization proteins in Streptococcus pneumoniae using novel fluorescent reporter
976 systems. Mol Microbiol. 2009;74(2):395–408.

977 73. Berg KH, Biørnstad TJ, Straume D, Håvarstein LS. Peptide-Regulated Gene Depletion
978 System Developed for Use in Streptococcus pneumoniae. J Bacteriol. 2011 Sep
979 13;193(19):5207–15.

980 74. Martin B, Garcia P, Castanié MP, Claverys JP. The recA gene of Streptococcus pneumoniae
981 is part of a competence-induced operon and controls lysogenic induction. Mol
982 Microbiol. 1995;15(2):367–79.

983 75. van Raaphorst R, Kjos M, Veening JW. Chromosome segregation drives division site
984 selection in Streptococcus pneumoniae. Proc Natl Acad Sci. 2017 Jul 18;114(29):E5959–
985 68.

986 76. Tsui HCT, Joseph M, Zheng JJ, Perez AJ, Manzoor I, Rued BE, et al. Negative regulation of
987 MurZ and MurA underlies the essentiality of GpsB- and StkP-mediated protein
988 phosphorylation in Streptococcus pneumoniae D39. Mol Microbiol. 2023;120(3):351–83.

989 77. Perez AJ, Lamanna MM, Bruce KE, Touraev MA, Page JE, Shaw SL, et al. Elongasome core
990 proteins and class A PBP1a display zonal, processive movement at the midcell of
991 Streptococcus pneumoniae. Proc Natl Acad Sci. 2024 Jun 18;121(25):e2401831121.

78. Moore DA, Whatley ZN, Joshi CP, Osawa M, Erickson HP. Probing for Binding Regions of the FtsZ Protein Surface through Site-Directed Insertions: Discovery of Fully Functional FtsZ-Fluorescent Proteins. J Bacteriol. 2016 Dec 13;199(1):10.1128/jb.00553-16.